PNAS RESEARCH ARTICLE | APPLIED BIOLOGICAL SCIENCES

Self-adjuvanting α-helical polypeptide simultaneously delivers neoantigen mRNAs and activates dendritic cells to eradicate tumors

Joonsu Han[a,1], Jiadiao Zhou[a,1], Abhisek Dwivedy[b,1], Tianrui Xue[a], Rimsha Bhatta[a], Yusheng Liu[a], Daniel Nguyen[b], Yang Bo[a], Yueji Wang[a], Xin Wang[b], Meng Xu[a], Matthew Berry[c], Keith Bailey[d], Joseph Irudayaraj[a,b,e,f], Jian Liu[g], Qian Chen[a,h,i,j], Shuming Nie[a,b,k], Xing Wang[b,h,l,2], and Hua Wang[a,b,e,f,i,j,l,2]

Affiliations are included on p. 11.

Edited by Jeffrey Alan Hubbell, New York University, New York, NY; received March 5, 2025; accepted March 19, 2026

mRNA-based vaccines have demonstrated tremendous success during the era of COVID-19, but its therapeutic potential for treating cancer, especially poorly immunogenic solid tumors, remains largely underachieved. Herein, we report a class of self-adjuvanting α-helical polypeptides that can dramatically improve the antitumor efficacy of tumor neoantigen-encoding mRNAs. The α-helical polypeptides can facilitate the intracellular delivery of mRNAs into dendritic cells (DCs), simultaneously activate DCs by regulating NF-κB and IRF pathways, and improve the ability of dendritic cells to process and present mRNA-encoded neoantigens. Molecular docking and simulation results also confirm the stable complexation between mRNA and α-helical polypeptides. The conceived polyplex, upon subcutaneous administration, can migrate to the draining lymph nodes and transfect and activate DCs in the lymph nodes, resulting in superior neoantigen-specific cytotoxic T lymphocyte response in vivo. Compared to conventional lipoplexes or SM102 lipid nanoparticle-based mRNA vaccines that yield 0% tumor-free survival, the polyplex yields 83.3% and 33.3% tumor-free survival against E.G7-OVA lymphoma and 4T1 triple negative breast cancer, respectively, among the best antitumor efficacy reported to date for mRNA cancer vaccines. The polyplex also reprograms the immunosuppressive tumor microenvironment, by stimulating and enriching DCs, M1-phenotype CD86$^+$ macrophages, and CD8$^+$ T cells in the tumors. We also observed the upregulated expression of Programmed Death-1 (PD-1) by intratumoral CD8$^+$ T cells and PD-L1 by 4T1 tumor cells after polyplex treatment and further demonstrated the synergistic effect between polyplex vaccine and anti-PD-1 therapy. Our polyplex system provides a facile and generalizable approach to developing robust mRNA-based cancer vaccines.

mRNA vaccine | polypeptide | cancer | immunotherapy | adjuvant

Significance

Messenger RNA (mRNA)-based cancer vaccines have long been sought, but are limited by the modest therapeutic efficacy. One central challenge lies in the development of mRNA carriers that not only facilitate the expression of mRNA-encoded tumor antigens in dendritic cells (DCs) but can also appropriately activate DCs in a timely manner. Herein, we report self-adjuvanting α-helical polypeptides that can 1) stabilize mRNA, 2) facilitate intracellular delivery of mRNAs via temporary disruption of DC membrane, and 3) meanwhile activate DCs by regulating Nuclear Factor-kappa B (NF-κB) and Interferon Regulatory Factor (IRF) pathways. The conceived polyplex yields 83.3% and 33.3% tumor-free survival against E.G7 lymphoma and 4T1 triple negative breast cancer. Our polyplex system provides an alternative to develop robust mRNA cancer vaccines.

Cancer immunotherapies have shown the promise to cure cancer by boosting the body's immune system to better combat cancer, especially with the success of checkpoint blockades and chimeric antigen receptor T cell therapy (1–6). Among them, therapeutic cancer vaccines, which function by modulating antigen-presenting cells [e.g., dendritic cells (DCs)] with tumor-associated antigens and adjuvants, have shown the ability to elicit tumor-specific cytotoxic T lymphocyte (CTL) responses with well-documented safety profiles in various clinical trials, but are limited by the modest therapeutic benefit to date (7–14). Various types of cancer vaccines including whole tumor cell vaccines, tumor exosome vaccines, mRNA vaccines, DNA vaccines, nanomaterial vaccines, and biomaterial scaffold vaccines have been developed to date (10–14). Among them, mRNA vaccines that encode tumor-specific neoantigens have emerged as a promising platform for clinical translation (15–18), especially in light of the tremendous success of mRNA vaccines in the era of COVID-19. Indeed, multiple mRNA vaccines are being tested for treating melanoma, colon cancer, lung cancer, and other types of cancer in clinical trials (19–21). However, developing mRNA vaccines with potent tumor-specific CTL response and antitumor efficacy, especially for poorly immunogenic solid tumors, remains a significant challenge (22–24).

To generate potent CTL response, mRNA vaccines need to induce efficient uptake and processing of antigen-encoding mRNAs by DCs, and meanwhile properly activate DCs to facilitate the presentation of antigens via major histocompatibility complexes (MHC) (17, 25). Lipid nanoparticle (LNP) is one of the most successful delivery vehicles for mRNAs and other nucleic acids to date, as evidenced by the tremendous success with COVID-19 vaccines. LNPs encapsulating tumor antigen-encoded mRNAs have also been

This article is a PNAS Direct Submission.

[1]J.H., J.Z., and A.D. contributed equally to this work.

[2]To whom correspondence may be addressed. Email: xingw@illinois.edu or huawang3@illinois.edu.

This article contains supporting information online at https://www.pnas.org/lookup/suppl/doi:10.1073/pnas.2504976123/-/DCSupplemental.

Published April 15, 2026.

actively explored for cancer treatment (26–29). For example, LNPs encapsulating TRP2 or gp100 mRNA were developed for the treatment of B16F10 melanoma (26–28). However, the therapeutic benefit of mRNA-LNP cancer vaccines, especially for the treatment of solid tumors such as triple negative breast cancer (TNBC), is still limited, likely due to the inadequate activation of DCs in a timely manner (30–32). Ongoing and future efforts in the screening of LNPs for optimal modulation of DCs hold promise to further improve the CTL response and antitumor efficacy of mRNA-LNP vaccines (27, 33, 34). Alternatively, conventional nucleic acid delivery vehicles such as cationic polymers have also been actively explored for the delivery of tumor antigen-encoding mRNAs in the context of cancer treatment (35–38). Polymeric carriers of mRNAs could have a simpler structure than hybrid nanoparticles, easy complexation with mRNAs with precisely defined N/P ratios, and versatile chemical structures, possessing great potential for developing robust mRNA cancer vaccines. However, existing polyplex-based cancer vaccines have shown limited therapeutic efficacy in general (35–38).

Here we report a class of α-helical polypeptides that can serve as a self-adjuvanting mRNA delivery vehicle to develop potent mRNA cancer vaccines, and highlight the importance for an mRNA carrier to properly activate DCs in a timely manner. The cationic α-helical polypeptides can condense and stabilize neoantigen-encoding mRNAs, facilitate the cell uptake of mRNAs by DCs, and meanwhile activate DCs by upregulating the NF-κB and IRF pathways, resulting in significantly improved intracellular processing and presentation of mRNA-encoded antigens by DCs. The polyplexes of α-helical polypeptides and neoantigen-encoding mRNAs can be synthesized via a simple mixing step, and upon subcutaneous injection, can elicit potent neoantigen-specific CTL response and therapeutic efficacy against multiple types of tumors including E.G7-OVA lymphoma and 4T1 TNBC. This polyplex system provides a facile and generalizable platform for developing enhanced mRNA-based vaccines for treating a range of cancers.

Results

Development of Self-Adjuvanting α-Helical Polypeptides. In view of the cell-penetrating property of certain cationic peptides (39–42), we envision cationic α-helical polypeptides (43–45) that can interact with negatively charged cell membranes could provide a "danger signal" to DCs and induce the activation of DCs. To demonstrate this hypothesis, we synthesized a type of water-soluble α-helical polypeptide via the ring-opening polymerization of 4-propargyloxybenzyl-L-glutamic acid-*N*-carboxyanhydride (POB-NCA) and postpolymerization click reaction with azidohexylguanidine (Fig. 1*A*). The polypeptide with a degree of polymerization of 50, named $PPOB_{50}$-G, was well characterized by the NMR spectrometry (*SI Appendix*, Figs. S1–S3). Per the circular dichroism (CD) spectrometry, $_{L}$-type and $_{D}$-type $PPOB_{50}$-G exhibited an α-helical structure, evidenced by the characteristic peaks at 208 and 222 nm (Fig. 1*B*) (44, 46–49). In contrast, $_{D,L}$-$PPOB_{50}$-G synthesized via the polymerization of a mixture of $_{L}$- and $_{D}$-type monomers showed a random-coil structure (Fig. 1*B*). It is noteworthy that $_{D,L}$-$PPOB_{50}$-G did not exhibit a 100% random-coil structure (Fig. 1*B*), likely due to the presence of $_{L}$- and $_{D}$-repeats in the polymer backbone. To study the adjuvanting effect of $PPOB_{50}$-G, murine bone marrow derived DCs (BMDCs) were incubated with $_{L}$-$PPOB_{50}$-G, $_{D}$-$PPOB_{50}$-G, $_{D,L}$-$PPOB_{50}$-G, CpG, and PBS, respectively for 16 h. Compared to untreated cells, DCs treated with $PPOB_{50}$-G showed a significantly higher expression of CD86 and MHCII, two prominent activation markers of DCs (50, 51) (Fig. 1 *C–F*). $PPOB_{50}$-G also upregulated the expression of CD40 and CCR7, which were reported to increase with the activation status of DCs (52, 53), in comparison with untreated DCs (Fig. 1 *G–J*). Compared to $_{D,L}$-$PPOB_{50}$-G, $_{L}$-$PPOB_{50}$-G resulted in higher expression levels of CD86, MHCII, CD40, and CCR7 (Fig. 1 *C–J*), indicating the contribution of α-helical structure to DC activation. In an effort to understand the mechanism underlying the enhanced activation status of polyplex-treated DCs, we analyzed the intracellular expression levels of NF-κB, p-NF-κB, IRF3, p-IRF3, IRF7, p-IRF7, and MyD88, which were shown to be associated with the simulation of toll-like receptors (TLRs) on the surface of DC membrane or endosomes. Compared to DCs treated with PBS or $_{D,L}$-$PPOB_{50}$-G, DCs treated with $_{L}$-$PPOB_{50}$-G exhibited an upregulated expression of NF-κB, p-NF-κB, IRF3, p-IRF3, IRF7, p-IRF7, and MyD88 (Fig. 1*K*). Indeed, $_{L}$-$PPOB_{50}$-G induced a similar expression level of these markers to CpG, a commonly used TLR9 agonist (Fig. 1*K*). Interestingly, in addition to CpG-type stimulation, $_{L}$-$PPOB_{50}$-G also upregulated the expression level of p-STING and cGAS (Fig. 1*K*), indicating the activation of the STING pathway.

α-Helical $PPOB_{50}$-G Improves Intracellular Delivery and Processing of mRNAs. We next studied whether $PPOB_{50}$-G can facilitate the delivery of mRNAs into DCs and improve the mRNA transfection efficiency in DCs. Cationic $_{L}$-$PPOB_{50}$-G could form stable nanosized complexes with eGFP-encoding mRNAs via simple mixing (Fig. 1 *L* and *M*). The size of formed polyplexes decreased while zeta potential increased with the N/P ratio, as expected (Fig. 1*M* and *SI Appendix*, Fig. S4*A*). The formed polyplexes are stable under physiological conditions for 72 h (*SI Appendix*, Fig. S4*B*). To track the cell uptake efficiency of mRNA, mRNA was stained with SYBR Green II and then complexed with $PPOB_{50}$-G. Compared to free mRNAs, $_{L}$-$PPOB_{50}$-G polyplexes showed a significantly higher uptake efficiency by DCs, as determined by flow cytometry (Fig. 1*N*). Confocal images also confirmed the enhanced uptake of $_{L}$-$PPOB_{50}$-G polyplexes by DCs in comparison with free mRNA (Fig. 1*O*). We also confirmed the enhanced DC uptake of Cy5-tagged eGFP mRNA polyplexes than free mRNAs (*SI Appendix*, Fig. S4 *C* and *D*). To assess the endosomal colocalization of polyplexes, DCs were incubated with Cy5-labeled mRNA polyplexes for 4 h and stained with LysoTracker and DAPI. Confocal images showed a partial colocalization of Cy5 with Lysotracker, with some Cy5 signal observed outside the LysoTracker-positive regions (*SI Appendix*, Fig. S4*E*). We envision that a portion of polyplexes are likely internalized by DCs via endosomes and the interactions between polyplexes and cell membranes can facilitate the uptake process. The mRNA loading efficiency of $_{L}$-$PPOB_{50}$-G increased with the N/P ratio, and an N/P ratio of 10/1 resulted in ~100% eGFP mRNA loading efficiency (*SI Appendix*, Fig. S4*F*). To assess the mRNA transfection efficiency, BMDCs were incubated with the polyplexes of eGFP mRNA and $_{L}$-$PPOB_{50}$-G at varied N/P ratios, SM-102 LNPs encapsulating eGFP mRNA (6/1 N/P ratio), lipoplexes of eGFP mRNA and lipofectamine 3000 (10/1 N/P ratio), free eGFP mRNA, or PBS for 16 h, and the expression of eGFP in DCs was analyzed via fluorescence microscopy and flow cytometry. As expected, free mRNA failed to express any detectable eGFP in DCs (Fig. 1 *P–R*). Compared to lipoplexes and LNPs, polyplexes resulted in significantly higher expression of eGFP in DCs, and the transfection efficiency of polyplexes increased with the N/P ratio (Fig. 1 *P–R*). Compared to $_{D,L}$-polyplexes, $_{L}$-polyplexes also induced significantly higher eGFP expression, substantiating the contribution of the α-helical structure to enhance mRNA delivery (*SI Appendix*, Fig. S4 *G* and *H*).

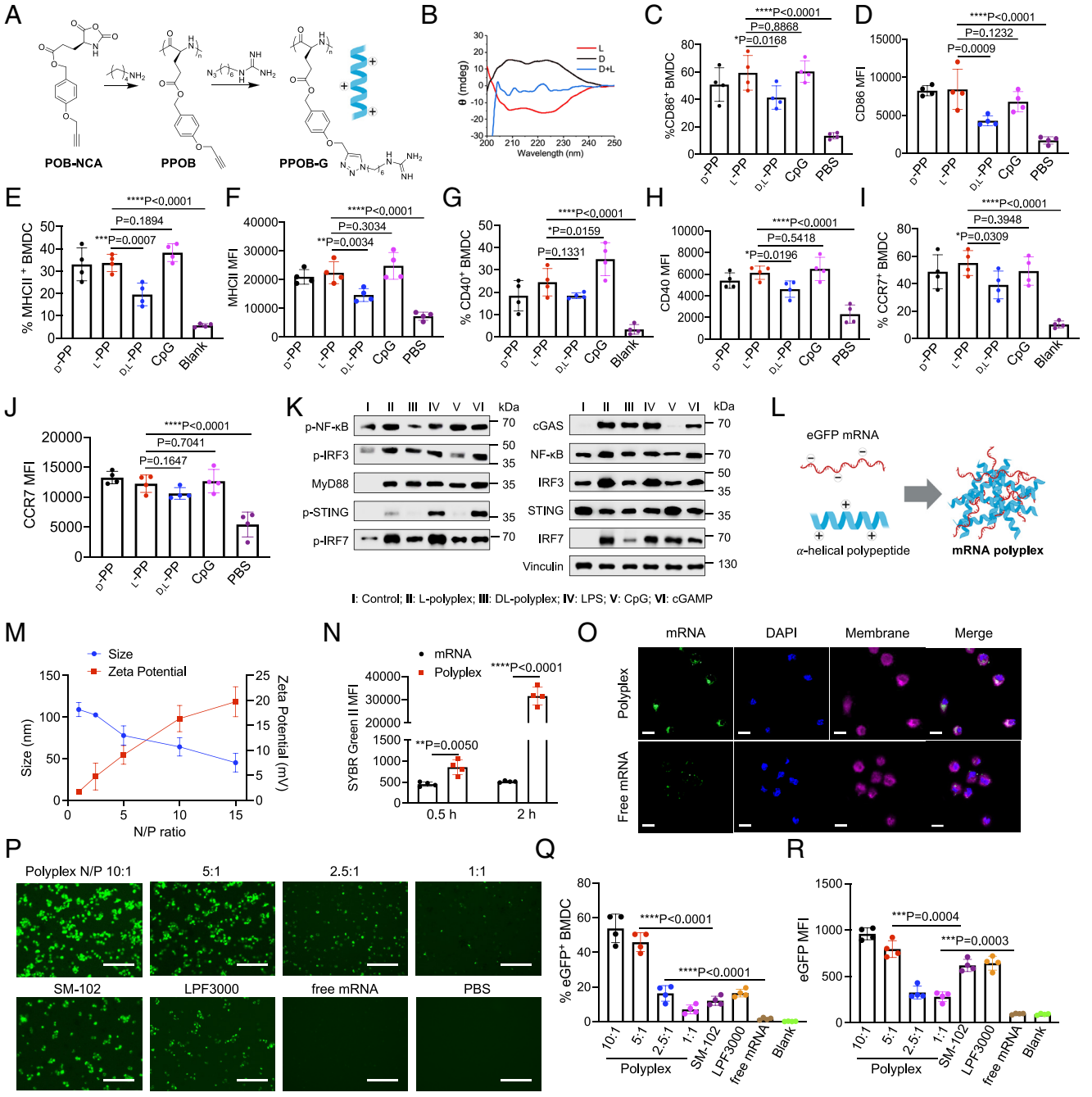

Fig. 1. α-Helical polypeptide PPOB-G activates DCs by stimulating NF-κB, IRF, and cGAS–STING pathways and improves the internalization and expression of mRNAs by DCs. (*A*) Synthetic route of α-helical polypeptide, PPOB-G. (*B*) CD spectra of $_{L}$-PPOB$_{50}$-G, $_{D}$-PPOB$_{50}$-G, and $_{D,L}$-PPOB$_{50}$-G. (*C*–*J*) DCs were incubated with $_{L}$-PPOB$_{50}$-G, $_{D}$-PPOB$_{50}$-G, $_{D,L}$-PPOB$_{50}$-G, CpG, or PBS for 16 h. Shown are the expression levels of (*C* and *D*) CD86, (*E* and *F*) MHCII, (*G* and *H*) CD40, and (*I* and *J*) CCR7. (*K*) Western blot analysis of NF-κB, MyD88, and cGAS–STING pathways in BMDCs treated with PBS, $_{L}$-PPOB$_{50}$-G, $_{D,L}$-PPOB$_{50}$-G, LPS, CpG, and cGAMP, respectively for 16 h. Representative images from at least two independent experiments are shown. (*L*) Formation of polyplexes via the mixing of $_{L}$-PPOB$_{50}$-G and mRNA. (*M*) Size and zeta potential of polyplexes with different N/P ratios. (*N*) Mean SYBR Green II fluorescence intensity of DCs after 0.5 h or 2 h incubation with SYBR Green II tagged mRNA polyplex or free mRNA. (*O*) CLSM images of DCs after 2 h incubation with SYBR Green II tagged mRNA polyplex or free mRNA. (Scale bar, 100 μm.) (*P*) Fluorescence images of DCs after treatment with eGFP-encoding polyplexes of different N/P ratios, SM-102 LNP (6/1 N/P ratio), LPF3000 lipoplexes (10/1 N/P ratio), free eGFP mRNA, or PBS for 16 h. (Scale bar, 150 μm.) Also shown are (*Q*) percentages of eGFP^{+} DCs and (*R*) mean eGFP fluorescence intensity of DCs after treatment with eGFP-encoding polyplexes of different N/P ratios, SM-102 LNP (6/1 N/P ratio), LPF3000 lipoplexes (10/1 N/P ratio), free eGFP mRNA, or PBS for 16 h. The dose of eGFP mRNA was kept at 500 ng/mL. All the numerical data are presented as mean ± SD (one-way ANOVA with post hoc Fisher's LSD test was used; 0.01 < *P ≤ 0.05; **P ≤ 0.01; ***P ≤ 0.001; ****P ≤ 0.0001).

It is noteworthy that polyplexes (N/P ≤ 10/1) were well tolerated by DCs (*SI Appendix*, Fig. S4*I*). These experiments demonstrated the capability of α-helical $_{L}$-PPOB$_{50}$-G to stabilize mRNA, facilitate the internalization of mRNAs by DCs, and improve the transfection efficiency of mRNAs in DCs.

$_{L}$-PPOB$_{50}$-G Polyplex Shows Improved DC Activation and Antigen Presentation. We next studied whether the polyplex of $_{L}$-PPOB$_{50}$-G and SIINFEKL-encoding mRNAs can improve the antigen presentation efficiency of DCs (Fig. 2*A*). The mRNA encoding for SIINFEKL peptide was synthesized, purified, and validated via the

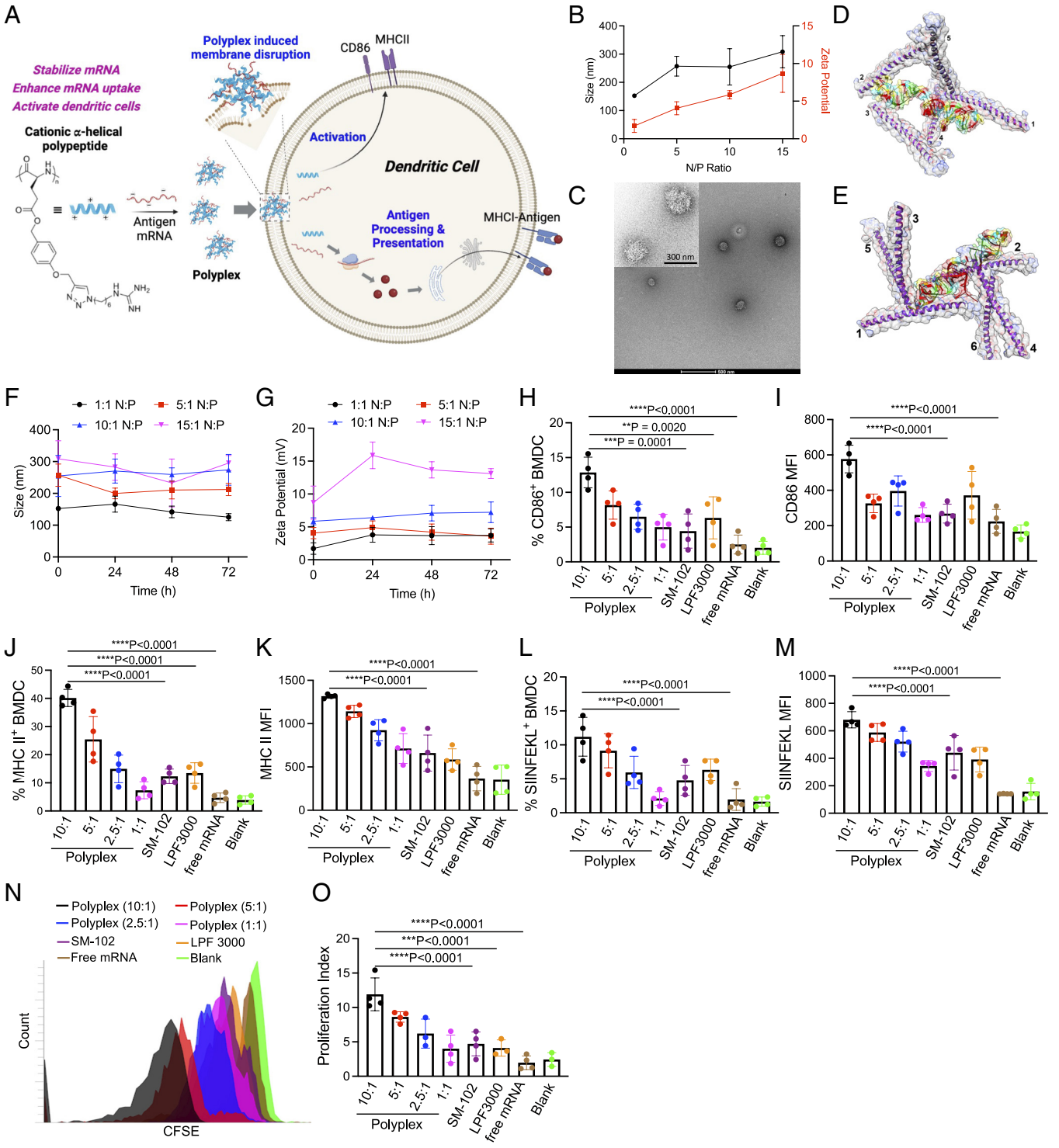

Fig. 2. Nanosized PPOB$_{50}$-G polyplex can activate DCs and improve the presentation of mRNA-encoded antigens by DCs. (*A*) Schematic illustration of self-adjuvanting α-helical polypeptides for simultaneous mRNA delivery and DC activation. On one hand, the cationic α-helical polypeptide can stabilize neoantigen-encoding mRNAs and facilitate intracellular delivery of mRNAs via its cell-penetrating property. On the other hand, the α-helical polypeptide can provide a danger signal to activate DCs and lead to improved neoantigen presentation by DCs. (*B*) Size and zeta potential of PPOB$_{50}$-G/SIINFEKL mRNA polyplex at different N/P ratios. (*C*) TEM image of PPOB$_{50}$-G/SIINFEKL mRNA polyplex (10/1 N/P ratio). (*D*) Multipeptide complex showing five PPOB$_{50}$-G peptides binding at different sites on SIINFEKL mRNA with a free energy of −56.71 kcal mol^{-1}. (*E*) Multipeptide complex showing six PPOB$_{50}$-G peptides binding at different sites on the SIINFEKL mRNA with a free energy of −64.29 kcal mol^{-1}. The order of docked peptides is represented in numbers. (*F*) Size of PPOB$_{50}$-G/SIINFEKL mRNA polyplex of varied N/P ratios over time in PBS. (*G*) Zeta potential of PPOB$_{50}$-G/SIINFEKL mRNA polyplex of varied N/P ratios over time in PBS. (*H–M*) BMDCs were treated with PPOB$_{50}$-G polyplexes at varied N/P ratios, SM-102 LNP (6/1 N/P ratio), LPF3000 lipoplexes (10/1 N/P ratio), or free mRNA with an mRNA concentration of 1 μg/mL for 16 h. The dose of SIINFEKL mRNA was kept at 500 ng/mL. (*H*) Percentages of CD86$^+$ DCs. (*I*) mean CD86 fluorescence intensity of DCs. Also shown are (*J*) % MHCII$^+$ DCs and (*K*) Mean MHCII fluorescence intensity. (*L*) Percentages of MHCI–SIINFEKL$^+$ DCs. (*M*) Mean MHCI–SIINFEKL fluorescence intensity of DCs. (*N* and *O*) Following the same treatment as in (*H–M*), BMDCs were cocultured with CFSE-stained OT-1 cells for 3 d. (*N*) Representative CFSE histograms of OT-1 cells. (*O*) Proliferation index of OT-1 cells after 3-d coculture with DCs. All numerical data in these figures are presented as mean ± SD (one-way ANOVA with post hoc Fisher's LSD test was used; 0.01 < **P* ≤ 0.05; ***P* ≤ 0.01; ****P* ≤ 0.001; *****P* ≤ 0.0001).

agarose gel electrophoresis (*SI Appendix*, Fig. S5*A* and Table S1). $_{L}$-PPOB$_{50}$-G polyplexes with a <10/1 N/P ratio showed minimal cytotoxicity toward BMDCs (*SI Appendix*, Fig. S5*B*). The average diameter of $_{L}$-PPOB$_{50}$-G/SIINFEKL mRNA polyplexes was 153 nm, 257 nm, 255 nm, and 309 nm for the N/P ratio of 1/1, 5/1, 10/1, and 15/1, respectively (Fig. 2*B*). The zeta potential of $_{L}$-PPOB$_{50}$-G/SIINFEKL mRNA polyplexes was 1.7 mV, 4.1 mV, 5.9 mV, and 8.7 mV for the N/P ratio of 1/1, 5/1, 10/1, and 15/1, respectively (Fig. 2*B*). TEM imaging also confirmed the formation of nanosized polyplexes (Fig. 2*C*). To develop a mechanistic understanding of how $_{L}$-PPOB$_{50}$-G interacts with mRNA and aids in its delivery, we performed computational structural modeling, docking, and molecular dynamics simulations. In the absence of an experimentally determined three-dimensional (3D) structure, ab initio structure modeling was utilized to generate the structure (*SI Appendix*, Fig. S6). The non-natural amino acid (NAA) structure generated ab initio exhibited less than 0.5 Å of RMSD in the minimization multidimensional scaling (MDS) (*SI Appendix*, Fig. S6*A*), suggesting a degree of stability in aqueous solvent (Movie S1). Upon successful generation of NAA structure and rotamer identification, the model for the 50-residue helical peptide ($_{L}$-PPOB$_{50}$-G) was generated (*SI Appendix*, Fig. S6*B*). The helical peptide exhibited strong interactions with chloride ions in the minimization MDS, and the negative charged regions buried toward the interior of the peptide while the positively charged regions were exposed to the peptide surface (Movie S2). The peptide also exhibited an overall change in helicity with a shorter pitch between turns. This suggests that in solution, the peptide exhibits a helical structure that borrows elements from both α and π type helices, which could be crucial for exposing the positively charged regions to the surface. To analyze the binding interactions between $_{L}$-PPOB$_{50}$-G and mRNA, we modeled the 3D structure of SIINFEKL mRNA (*SI Appendix*, Fig. S6*C*) and performed docking and MDS analysis. A one peptide-one RNA docking revealed five different binding modes (*SI Appendix*, Fig. S7*A*). Energy minimization of the binding modes revealed the following binding free energies: −22.69, −19.17, −18.94, −17.8, and −12.83 kcal mol^{-1}. The complex with the lowest binding free energy (*SI Appendix*, Fig. S7*B*) was further analyzed by minimization MDS. We observed strong overall stabilization of the complex with an increase in H-bonds from 29 to 44. Additionally, multiple ionic interactions and salt bridge interactions were observed between the mRNA and $_{L}$-PPOB$_{50}$-G (*SI Appendix*, Fig. S7 *C* and *D*). The final free energy of the complex post-MDS was calculated as −37.11 kcal mol^{-1} indicating a stable complex formation. The MDS also revealed that the negatively charged RNA backbone moved closer to the positively charged surface of the $_{L}$-peptide indicating a strong binding affinity (Movie S3). Taken together, these results suggest that the $_{L}$-peptide/mRNA complex is highly stable, more so than either of the interacting moieties in solution independently.

We next used sequential computational docking to determine the possible number of peptides bound to each SIINFEKL mRNA. We chose the original lowest energy structure (−22.69 kcal mol^{-1}) and performed docking of this mRNA–peptide complex to another peptide molecule. Subsequently the lowest energy complex with one RNA and two peptides was chosen and docked to a new peptide molecule. This was repeated until no accessible surface area for binding on the mRNA molecule remained. Our sequential docking analysis revealed two final complexes. The first complex had a free energy of −56.71 kcal mol^{-1}, with five peptides bound to a single mRNA (Fig. 2*D*). The second complex with a free energy of −64.29 kcal mol^{-1} exhibited six peptides interacting with one mRNA (Fig. 2*E*). These data suggest that the possible molar ratio of RNA to $_{L}$-peptide for forming a stable complex is 1:5 or 1:6. This aligns with our stability tests that polyplexes with an N/P ratio of 5/1 or 10/1 exhibited excellent stability under physiological conditions, as evidenced by the minimal change of diameter and zeta potential over 72 h (Fig. 2 *F* and *G*).

Prior to the antigen presentation test, we examined the DC-activating effect of polyplexes by incubating DCs with polyplexes, mRNA-LNP, lipoplexes, free mRNA, or PBS for 16 h. Compared to cells treated with mRNA-LNP, lipoplexes, or free mRNA, DCs treated with the polyplexes at an N/P ratio of 10/1 showed a significantly upregulated expression of CD86, MHCII, and CD80 (Fig. 2 *H*–*K* and *SI Appendix*, Fig. S8 *A*–*E*). In an effort to understand the underlying mechanism, we also treated BMDCs from STING-knockout (STING$^{-/-}$) mice and wild type (WT) Balb/c mice with polyplexes (SIINFEKL mRNA; N/P = 10/1). BMDCs from STING$^{-/-}$ or WT mice exhibited similar background expression levels of CD86, MHCII, and CD40 (*SI Appendix*, Fig. S9 *A*–*C*). Different from WT BMDCs that showed a significantly upregulated expression of CD86, MHCII, and CD40 in the polyplex group, STING$^{-/-}$ BMDCs showed negligible differences between polyplex and PBS groups (*SI Appendix*, Fig. S9 *A*–*C*), indicating the involvement of cGAS–STING signaling in polyplex-mediated activation of DCs. To further support the involvement of cGAS–STING signaling in polyplex-mediated activation of DCs, we also evaluated mitochondrial stress and DNA damage in BMDCs following polyplex treatment. Compared to BMDCs treated with free mRNA or PBS, polyplex-treated BMDCs showed an increased mitochondrial superoxide level (*SI Appendix*, Fig. S10 *A* and *B*), a reduced mitochondrial membrane potential (*SI Appendix*, Fig. S10*C*), and an elevated γH2AX (Ser139) signal (*SI Appendix*, Fig. S10 *D* and *E*), indicating that polyplex treatment can induce mitochondrial stress and DNA damage in BMDCs. In addition to the surface activation markers, we also examined the cytokine release profiles of BMDCs treated with $_{L}$-PPOB$_{50}$-G/SIINFEKL mRNA polyplexes, $_{L}$-PPOB$_{50}$-G, free SIINFEKL mRNA, or PBS. Compared to free mRNA or PBS, BMDCs treated with polyplexes showed an enhanced release of GM-CSF, CCL17, and CCL5 (*SI Appendix*, Fig. S11 *A* and *B*). These data demonstrated that the polyplex of $_{L}$-PPOB$_{50}$-G and mRNA, similar to the polypeptide itself, can induce the activation of DCs. In consistence with the DC-activating effect, the polyplexes resulted in significantly higher expression of MHCI–SIINFEKL complexes on DCs in comparison with mRNA-LNP, lipoplexes, or free mRNA (Fig. 2 *L* and *M*). To confirm the improved antigen presentation of polyplex-treated DCs and further evaluate whether polyplex-treated DCs can better stimulate SIINFEKL-specific CD8^{+} cells, DCs were cocultured with CFSE-stained OT-1 cells for 3 d. Compared to DCs pretreated with mRNA-LNP, lipoplexes or free mRNA, DCs pretreated with $_{L}$-PPOB$_{50}$-G polyplexes at an N/P ratio of 10/1 resulted in the significantly improved proliferation of OT-1 cells (Fig. 2 *N* and *O*). It is noteworthy that polyplex-pretreated DCs did not induce the exhaustion of OT-1 cells, as evidenced by the negligible change in the expression levels of PD-1, CTLA-4, and LAG-3 on OT-1 cells (*SI Appendix*, Fig. S12 *A*–*C*). In contrast, lipoplexes notably upregulated the expression of PD-1 and CTLA-4 by OT-1 cells (*SI Appendix*, Fig. S12 *A*–*C*). Together, these experiments demonstrated that $_{L}$-PPOB$_{50}$-G/mRNA polyplexes with an N/P ratio of 5:1 to 10:1 are stable, can induce the activation of DCs, and facilitate the processing and presentation of mRNA-encoded antigens by DCs.

$_{L}$-PPOB$_{50}$-G Polyplex Modulates DCs in Lymph Nodes and Results in Robust CTL Response. We next aimed to study the CTL response of the polyplexes of $_{L}$-PPOB$_{50}$-G and antigen-encoding mRNAs at an N/P ratio of 10/1 (Fig. 3*A*). Prior to that, we first studied whether subcutaneously injected polyplexes can migrate to lymph nodes and transfect DCs in the lymph nodes. The polyplexes of $_{L}$-PPOB$_{50}$-G and eGFP-encoding mRNAs at an N/P ratio of 10/1 were subcutaneously injected into the flank of C57BL/6 mice, and tissues at the injection site and draining lymph nodes (dLN) were harvested for the analysis of eGFP-expressing DCs at 12, 24, 48, and 72 h, respectively. At 12 h, 6.9% DCs in the dLN were eGFP-positive, which increased to 16.0% at 24 h and 20.0% at 48 h (Fig. 3 *B* and *C*), demonstrating the high efficiency of subcutaneously injected polyplexes to transfect DCs in the dLN. Despite showing a decrease after 48 h, the percentage of eGFP$^+$ DCs in the lymph nodes stayed at 14.4% at 72 h (Fig. 3 *B* and *C*). We also confirmed the successful transfection of DCs at the injection site of polyplexes, albeit with a lower percentage of eGFP$^+$ DCs than in the dLN (Fig. 3*D*). The decrease of eGFP expression over time at the injection site aligns with the gradual migration of polyplexes into the dLN (Fig. 3*D*). To confirm the ability of the subcutaneously administered polyplexes to directly migrate to DCs in the dLN, in a separate study, we injected Cy5-tagged, eGFP-encoding polyplexes into the flank of C57BL/6 mice and analyzed Cy5$^+$ DCs in the dLN, nondraining lymph nodes (ndLN), and skin tissues at the injection site 4 h later. A significantly higher Cy5 signal was detected in the dLN, while negligible differences between ndLN and the injection site were observed (*SI Appendix*, Fig. S13*A*). Further, we analyzed Cy5$^+$ fractions among CD103$^+$ DCs and CD103$^-$ DCs. CD103$^-$ DCs in dLN exhibited a higher Cy5 signal than CD103$^-$ DCs in ndLN (*SI Appendix*, Fig. S13*B*). However, CD103$^+$ DCs in dLN and ndLN showed negligible difference in Cy5 signal (*SI Appendix*, Fig. S13*C*). Together, these results demonstrated that polyplexes are able to directly drain to the lymph nodes and are taken up by DCs in the lymph nodes. In addition to transfecting DCs, polyplexes also upregulated the expression levels of CD86 and MHCII on the surface of DCs in the lymph nodes and injection site (Fig. 3 *E* and *F*), indicating the enhanced activation status of DCs as a result of polyplex treatment.

The excellent ability of polyplexes to transfect and activate DCs in the dLN encouraged us to explore the CTL response and antitumor efficacy of SIINFEKL-encoding polyplexes. C57BL/6 mice were subcutaneously injected with polyplexes, lipoplexes, free mRNA, or PBS, followed by the analysis of SIINFEKL-specific CD8$^+$ T cells in peripheral blood mononuclear cells (PBMCs) (Fig. 3*G*). At 10, 14, and 20 d postvaccination, a higher frequency of SIINFEKL-specific CD8$^+$ T cells, as determined via tetramer staining or ex vivo IFN-γ restimulation, was consistently detected in mice treated with polyplexes than mice treated with free mRNA (Fig. 3 *H–J* and *L–N*). Following a booster vaccine at 35 d, a significantly higher number of SIINFEKL-specific CD8$^+$ T cells was still detected in polyplex-treated mice than in mice treated with free mRNA (Fig. 3 *K* and *O*). In the following prophylactic tumor study, $_{L}$-polyplexes resulted in the reduced tumor growth rate and prolonged animal survival than $_{D,L}$-polyplexes, lipoplexes, or free mRNA (Fig. 3 *P* and *Q* and *SI Appendix*, Fig. S14 *A–F*).

We next studied the applicability of the $_{L}$-PPOB$_{50}$-G polyplex system to develop enhanced neoantigen mRNA vaccines against 4T1 TNBC, a notoriously tough solid tumor resistant to existing immunotherapy. The mRNAs encoding for four 4T1 tumor-specific neoantigens (4T1-26, 4T1-31, 4T1-32, and 4T1-35) (15) were synthesized, purified, and validated via the agarose gel electrophoresis (*SI Appendix*, Fig. S5*A* and Table S1). We then complexed them (1:1:1:1 ratio for the four neoantigen mRNAs) with $_{L}$-PPOB$_{50}$-G to compose the cancer vaccine. Balb/c mice were subcutaneously injected with polyplexes or mRNA-LNP or free mRNAs on day 0 (Fig. 4*A*). On Day 7, a significantly higher frequency of neoantigen-specific CD8$^+$ T cells in PBMCs was detected in the polyplex group than in other groups (Fig. 4 *B* and *F*). This improvement was consistently detected on Days 14 and 21 (Fig. 4 *C, D, G,* and *H*). After a booster dose of vaccine on Day 35, polyplex-treated mice still showed a significantly higher number of 4T1 neoantigen-specific CD8$^+$ T cells than mice treated with mRNA-LNP or free mRNA (Fig. 4 *E* and *I* and *SI Appendix*, Fig. S15 *B* and *C*). In the subsequent prophylactic study, the polyplex led to significantly improved 4T1 tumor inhibition and animal survival in comparison with mRNA-LNP or free mRNAs (Fig. 4 *J* and *K* and *SI Appendix*, Fig. S15 *D–H*). In a separate experiment, we also compared the CTL response of polyplexes and the lipoplexes of SIINFEKL mRNA and lipofectamine 3000 (*SI Appendix*, Fig. S16*A*). At 7, 14, 21, and 35 d postvaccination, polyplexes induced a higher number of neoantigen-specific CD8$^+$ T cells in PBMCs than lipoplexes (*SI Appendix*, Fig. S16 *B–F*), and resulted in a better tumor control in the following prophylactic tumor study (*SI Appendix*, Fig. S16 *G–I*). These experiments substantiated the ability of $_{L}$-PPOB$_{50}$-G/mRNA polyplexes in orchestrating robust neoantigen-specific CTL response.

$_{L}$-PPOB$_{50}$-G Polyplex Shows Superior Therapeutic Antitumor Efficacy. We next studied the therapeutic efficacy of the polyplex vaccine against E.G7-OVA lymphoma and 4T1 TNBC. For the E.G7-OVA lymphoma model, we composed the polyplex vaccine by complexing $_{L}$-PPOB$_{50}$-G with SIINFEKL-encoding mRNA at an N/P ratio of 10/1. C57BL/6 mice were inoculated with E.G7-OVA tumor cells on Day 0 and divided into four groups: polyplex, lipoplex, free mRNA, and no treatment. On Days 6 and 13, vaccines were subcutaneously injected into the flank of mice (Fig. 5*A*). Free mRNA failed to exert any therapeutic benefit in comparison with the untreated groups (Fig. 5*B* and *SI Appendix*, Fig. S17 *A–E*). Compared to lipoplexes or free mRNA, $_{L}$-PPOB$_{50}$-G polyplexes resulted in the significantly reduced tumor growth rate and prolonged animal survival (Fig. 5 *B* and *C* and *SI Appendix*, Fig. S17 *A–E*). Indeed, polyplex vaccine was able to shrink established E.G7-OVA tumors and led to ~83.3% tumor-free survival, in sharp contrast with 0% for lipoplex vaccine or free mRNA vaccine (Fig. 5 *B* and *C* and *SI Appendix*, Fig. S17 *A–E*).

For the tough 4T1 TNBC model, we composed the polyplex vaccine by complexing $_{L}$-PPOB$_{50}$-G with mRNAs that encode 4T1 tumor-specific 4T1-26, 4T1-31, 4T1-32, and 4T1-35 neoantigens at an N/P ratio of 10/1. Balb/c mice were inoculated with 4T1 TNBC cells on Day 0 and divided into four groups: polyplex, lipoplex, free mRNA, and no treatment. Vaccines were subcutaneously administered on Days 6 and 13 (Fig. 5*D*). Both the polyplexes and lipoplexes resulted in improved therapeutic efficacy than free mRNAs (Fig. 5 *E* and *F* and *SI Appendix*, Fig. S18 *A–E*). Compared to lipoplexes that led to 0% tumor-free survival, polyplexes resulted in a slower tumor growth rate and 33.3% tumor-free survival (Fig. 5 *E* and *F* and *SI Appendix*, Fig. S18 *A–E*). It is noteworthy that the polyplex vaccine also managed to shrink the established 4T1 tumors between 7 and 14 d postvaccination (Fig. 5*F* and *SI Appendix*, Fig. S18 *A–F*). In separate experiments, we also compared the therapeutic efficacy of polyplexes and mRNA-SM102 LNP. Compared to mRNA-SM102 LNP, the polyplexes also resulted in significantly better tumor control and animal survival (Fig. 5*G* and *SI Appendix*, Fig. S19 *A–G*). To understand potential nonspecific immunostimulatory effects of polyplex vaccines, we also compared the efficacy of 4T1 neoantigen-encoded polyplexes with SIINFEKL-encoded

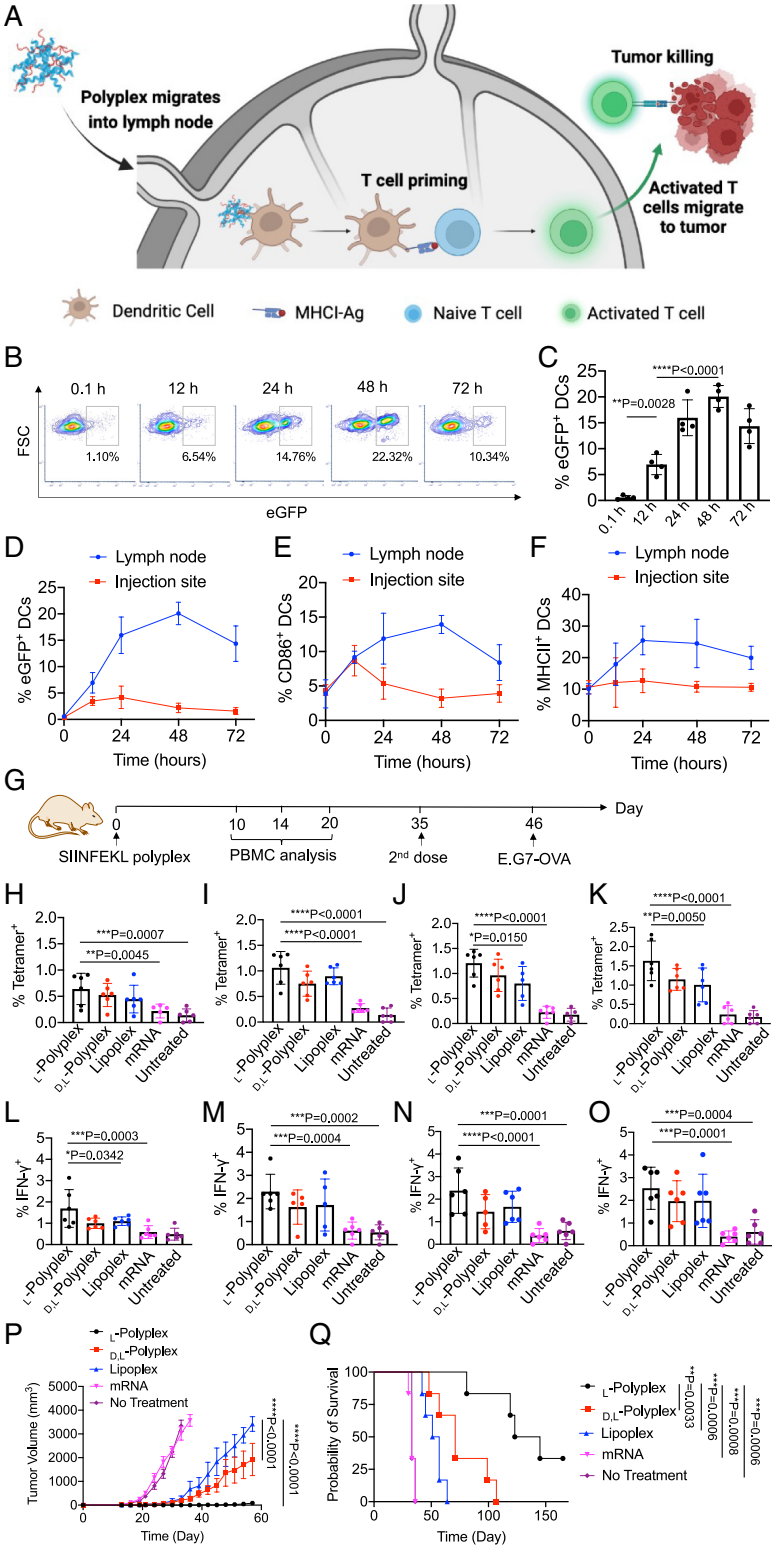

Fig. 3. $PPOB_{50}$-G polyplex efficiently transfects DCs in the dLN and results in persistent CTL response and prophylactic antitumor efficacy against E.G7-OVA lymphoma. (*A*) Subcutaneously administered polyplex vaccine can migrate to lymph nodes to modulate DCs, generating properly activated and neoantigen-presenting DCs for the elicitation of potent CTL response. (*B–F*) eGFP-encoding polyplexes (10/1 N/P ratio, 1 mg/kg eGFP mRNA) were subcutaneously injected into the flank of C57BL/6 mice, and dLN and skin tissues at the injection site were harvested at 0.1, 24, 48, and 72 h postinjection for analysis. (*B*) Representative FSC-eGFP FACS plots of $CD11c^+$ DCs in the dLN. (*C*) Percentages of $eGFP^+$ DCs in the dLN at 0.1, 24, 48, and 72 h, respectively postinjection of eGFP polyplexes. Also shown are percentages of (*D*) $eGFP^+$ DCs, (*E*) $CD86^+$ DCs, and (*F*) $MHCII^+$ DCs in the dLN and injection site at 0.1, 24, 48, and 72 h, respectively postinjection of eGFP polyplexes. (*G–Q*) Polyplexes, LPF3000 lipoplexes, or free mRNAs (1 mg/kg SIINFEKL mRNA) were injected on Days 0 and 35, followed by subcutaneous inoculation of *E*.G7-OVA tumor cells on Day 46. (*G*) Timeframe of the vaccination study. Shown are the percentages of SIINFEKL $tetramer^+$ cells among $CD8^+$ T cells in PBMCs on (*H*) Day 10, (*I*) Day 14, (*J*) Day 20, and (*K*) Day 45, respectively. (*L–O*) Percentages of IFN-γ^+ cells among $CD8^+$ T cells in PBMCs upon ex vivo restimulation with SIINFEKL peptide on (*L*) Day 10, (*M*) Day 14, (*N*) Day 20, and (*O*) Day 45, respectively. (*P*) Average E.G7-OVA tumor volume for each group during the prophylactic tumor study. (*Q*) Kaplan–Meier plots for all groups. All the numerical data are presented as mean ± SD except for (*P*) where data are presented as mean ± SEM (for *H–O*, one-way ANOVA with post hoc Fisher's LSD test was used; for *P*, two-tailed Welch's *t* test was used; for *Q*, the log-rank test was used; $0.01 < {}^*P \le 0.05$; $^{**}P \le 0.01$; $^{***}P \le 0.001$; $^{****}P \le 0.0001$).

polyplexes for treating 4T1 tumor (*SI Appendix*, Fig. S20*A*). 4T1 neoantigen polyplexes consistently showed a favorable antitumor effect, with a significantly reduced tumor growth rate in comparison with SIINFEKL polyplexes (*SI Appendix*, Fig. S20 *B–D*). While SIINFEKL polyplex induced a slightly slower tumor growth than the untreated group, negligible differences in the tumor volume was observed on Day 29 and beyond (*SI Appendix*, Fig. S20 *C* and *D*). These results confirmed the importance of using matched antigens for tumor treatment. Importantly, despite its augmented antitumor efficacy, the polyplex mRNA vaccine did not result in signs of toxicity in healthy tissues including the spleen, heart, kidney, liver, and lung (Fig. 5*H* and *SI Appendix*, Figs. S17*F* and S18*F* and Table S2). These experiments substantiated the superior therapeutic efficacy of polyplex vaccines against lymphoma and TNBC.

$_L$-$PPOB_{50}$-G Polyplex Reprograms the Tumor Microenvironment. We next studied the alteration of 4T1 tumor microenvironment as a result of vaccine treatment. Balb/c mice were inoculated with

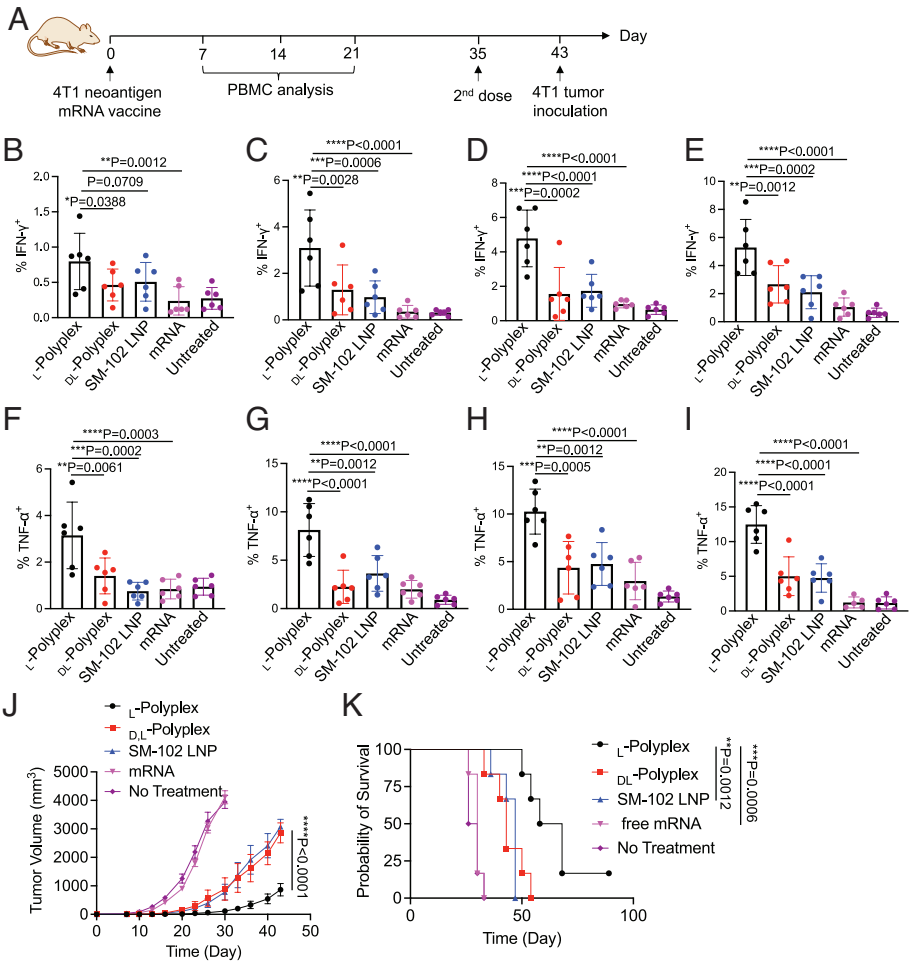

Fig. 4. $PPOB_{50}$-G polyplex elicits potent neoantigen-specific CTL response and prophylactic antitumor efficacy against 4T1 TNBC. (*A*) Timeframe of vaccination study. $_{L}$- polyplexes, $_{D,L}$-polyplexes, SM-102 LNP, free mRNAs, or PBS were subcutaneously injected on Days 0 and 35, followed by subcutaneous inoculation of 4T1 tumor cells on Day 43 (1 mg/kg mRNA; 4T1-26: 4T1-31: 4T1-32: 4T1-35 = 1:1:1:1). (*B–E*) Percentages of IFN-γ^+ cells among $CD8^+$ T cells in PBMCs upon ex vivo restimulation with 4T1 neoantigens on (*B*) Day 10, (*C*) Day 14, (*D*) Day 21, and (*E*) Day 42, respectively. (*F–I*) Percentages of TNF-α^+ cells among $CD8^+$ T cells in PBMCs upon ex vivo restimulation with 4T1 neoantigens on (*F*) Day 10, (*G*) Day 14, (*H*) Day 21, and (*I*) Day 42, respectively. (*J*) Average 4T1 tumor volume for each group during the prophylactic tumor study. (*K*) Kaplan–Meier plots for all groups. All the numerical data are presented as mean ± SD except for (*J*) where data are presented as mean ± SEM (for *B–I*, one-way ANOVA with post hoc Fisher's LSD test was used; for *J*, two-tailed Welch's *t* test was used; for *K*, the log-rank test was used; $0.01 < {*}P \le 0.05$; ${**}P \le 0.01$; ${***}P \le 0.001$; ${****}P \le 0.0001$).

4T1 TNBC on Day 0 and divided into four groups: polyplex, mRNA-SM102 LNP, free mRNA, and no treatment. Vaccines were subcutaneously administered on Days 6 and 13. On Day 27, tumors were harvested for immune analysis. Compared to untreated and free mRNA groups, polyplex and mRNA-LNP treatment increased the number of DCs and upregulated the expression of CD86 on the surface of DCs in the tumor microenvironment (Fig. 6 *A* and *B* and *SI Appendix*, Fig. S21). Compared to mRNA-LNP, polyplex treatment resulted in a higher number of $CD86^+$ DCs in the tumors (Fig. 6*B*). Polyplex treatment also induced a higher number of $CD86^+$ macrophages and a slightly higher number of $CD8^+$ T cells in the tumor microenvironment, in comparison with free mRNA or mRNA-LNP (Fig. 6 *C* and *D*). Compared to untreated mice, mice treated with polyplexes or mRNA-LNP exhibited a higher number of activated $CD69^+CD8^+$ T cells and a higher number ratio of $CD8^+$ T cells to regulatory T cells in the tumor microenvironment (Fig. 6 *E* and *F*). These results indicate that polyplexes can transfect and activate DCs in lymph nodes, followed by DC-mediated priming of tumor antigen-specific $CD8^+$ T cells, the infiltration of effector T cells into the tumor, and subsequent modulation of the tumor microenvironment. Interestingly, polyplexes also upregulated the expression of PD-1 on the surface of intratumoral $CD8^+$ T cells (Fig. 6*G*) and PD-L1 on the surface of 4T1 tumor cells (Fig. 6 *H* and *I*) in comparison with free mRNA or mRNA-LNP, likely as part of tumor evasion mechanisms in response to polyplex treatment. In view of this phenomenon, we next studied the combination therapy of polyplex and anti-PD-1 for 4T1 TNBC treatment. As expected, anti-PD-1 itself failed to exert any therapeutic benefit (Fig. 6*J*). Compared to polyplex alone, the combination of polyplex and anti-PD-1 showed an improved tumor control and animal survival (Fig. 6*J*), demonstrating their synergistic effect and providing a broad avenue to further improve the therapeutic efficacy of polyplexes.

Discussion

mRNA-based cancer vaccines has been an active and attractive area of research (54), given the recent success of mRNA vaccines during the era of COVID-19. Ideal carriers for antigen-encoding mRNAs can not only facilitate the expression of antigens in DCs, but should also properly activate DCs and induce the effective processing and presentation of expressed antigens by DCs (55). Herein we report the development of cationic α-helical polypeptides as a self-adjuvanting delivery vehicle for antigen-encoding mRNAs. The cationic α-helical polypeptide can condense and stabilize mRNAs, facilitate the internalization of mRNAs by DCs via its cell-penetrating property, and meanwhile increase the expression of activation markers (CD86, NHCII, CD40, and CCR7) on the surface of DCs by upregulating NF-κB, IRF, and STING pathways. $_{L}$-$PPOB_{50}$-G induced a similar expression level of these markers to CpG, a commonly used TLR9 agonist, but additionally activated STING pathway (p-STING and cGAS). These results indicate that α-helical $_{L}$-$PPOB_{50}$-G or $_{D}$-$PPOB_{50}$-G interacts with DC membranes and provides an overall danger signal to DCs. DCs, as a prominent type of innate immune cells, respond by upregulating multiple activation pathways. Compared to mRNA-SM102 LNPs or lipoplexes of lipofectamine 3000 and

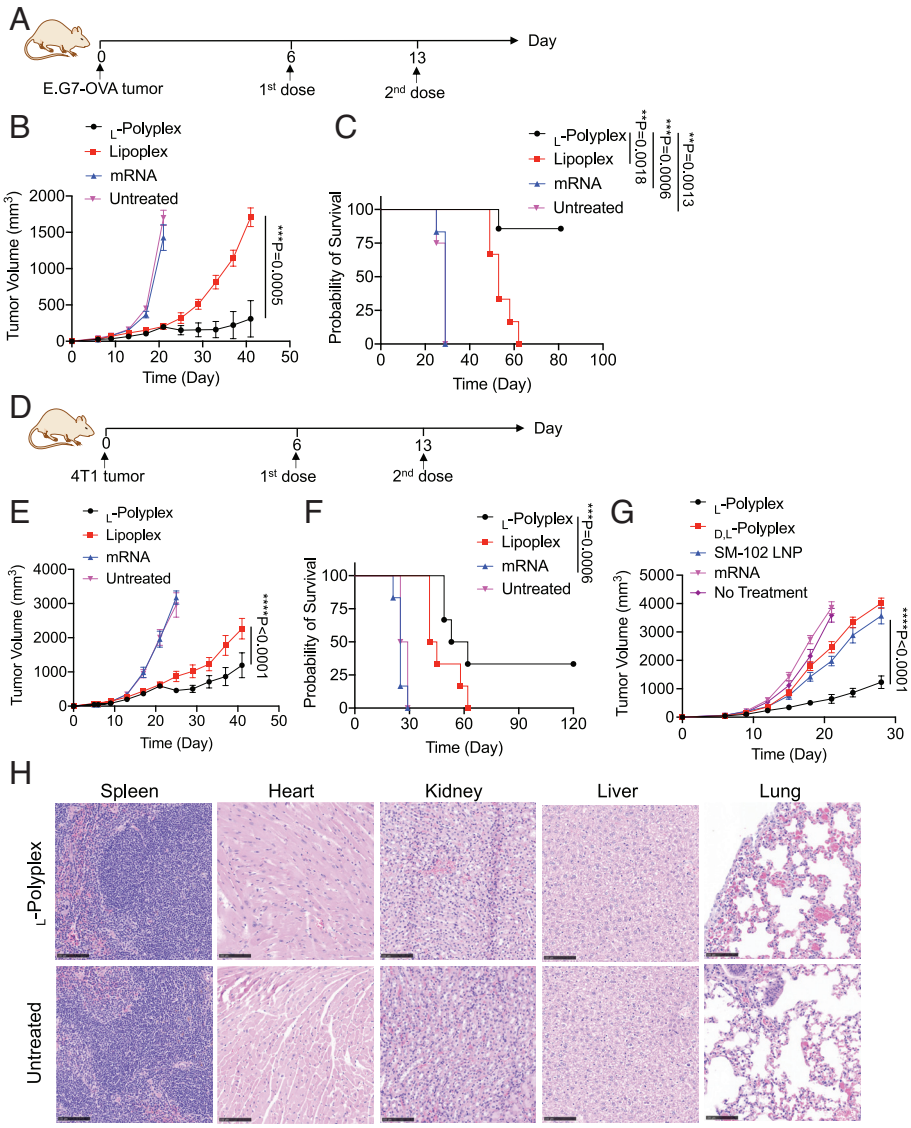

Fig. 5. $PPOB_{50}$-G polyplex exhibits superior therapeutic efficacy against E.G7-OVA lymphoma and 4T1 TNBC. (*A–C*) Therapeutic tumor study against E.G7-OVA tumor. (*A*) Timeframe of the efficacy study. E.G7-OVA tumor was inoculated on Day 0. Polyplexes, lipoplexes, or free mRNA were subcutaneously administered on Days 6 and 13 (1 mg/kg mRNA). (*B*) Average E.G7-OVA tumor volume over time for each group. (*C*) Kaplan–Meier plots for all groups. (*D–G*) Therapeutic tumor study against 4T1 TNBC. (*D*) Timeframe of the efficacy study. 4T1 tumor was inoculated on Day 0. Polyplexes, lipoplexes, or free mRNA (1 mg/kg mRNA, 4T1-26: 4T1-31: 4T1-32: 4T1-35 = 1:1:1:1) were administered on Days 6 and 13. (*E*) Average 4T1 tumor volume over time for each group. (*F*) Kaplan–Meier plots for all groups. (*G*) Average 4T1 tumor volume over time for each group. (Scale bar, 100 μm.) 4T1 tumor was inoculated on Day 0. Polyplexes, SM-102 LNP, or free mRNA (1 mg/kg mRNA, 4T1-26: 4T1-31: 4T1-32: 4T1-35 = 1:1:1:1) were administered on Days 6 and 13. (*H*) Representative images of H&E-stained tissue sections from mice treated with $_{L}$-polyplex or PBS. Numerical data in (*B*, *E*, and *G*) are presented as mean ± SEM (for *B*, *E*, and *G*, two-tailed Welch's *t* test was used; for *C* and *F*, the log-rank test was used; $0.01 < {}^{*}P \le 0.05$; $^{**}P \le 0.01$; $^{***}P \le 0.001$; $^{****}P \le 0.0001$).

mRNAs, the polyplexes can induce enhanced expression and presentation of mRNA-encoded antigens by DCs, and result in the significantly improved priming of antigen-specific $CD8^+$ T cells in vitro and in vivo. While polypeptides or poly(amino acids) have been previously reported as mRNA carriers and their nanoformulations could induce immunogenicity (56–58), our α-helical polypeptide itself can serve as an adjuvant and meanwhile a carrier of antigen-encoded mRNAs.

Neoantigens that result from genetic mutation of tumor cells are a promising source of tumor-specific antigens. However, the challenge to elicit potent and persistent neoantigen-specific CTL responses has curtailed the therapeutic efficacy of existing neoantigen-based cancer vaccines. We show that the polyplexes of α-helical $_{L}$-$PPOB_{50}$-G and mRNAs encoding 4T1 TNBC-specific neoantigens can elicit potent neoantigen-specific $CD8^+$ T cell response. In a therapeutic setting, the polyplex has also resulted in improved antitumor efficacy against 4T1 TNBC, a tough tumor model resistant to existing immunotherapies (59), in comparison with lipoplexes or free mRNAs. ~33% tumor-free survival was achieved with the polyplex vaccine, in sharp contrast to 0% for the lipoplex or free mRNAs. While exhibiting superior antitumor efficacy, the subcutaneously administered polyplexes did not induce any sign of notable toxicity to healthy tissues such as spleen, heart, kidney, liver, and lung. We envision the polyplex vaccine system can be universally applied to different types of neoantigen-encoding mRNAs for the treatment of different cancers. While the current study focuses on murine DCs and tumor models, future studies will examine the safety, CTL response, and antitumor efficacy of polyplexes in $CD34^+$ humanized mouse models. The facile manufacturing of the polyplexes, via simple mixing of polypeptides and mRNAs, also adds to the clinical translation potential of the polyplex vaccine platform.

Through a comprehensive set of studies, we show that subcutaneously injected polyplexes can migrate to the dLN and transfect and activate DCs in the lymph nodes to facilitate subsequent T cell priming processes. As a result, a significantly higher number of antigen-specific $CD8^+$ T cells can be generated in the lymph nodes, enter the systemic circulation, and accumulate in the tumor and eventually reprogram the tumor microenvironment, by stimulating and enriching DCs, M1-phenotype $CD86^+$ macrophages, and $CD8^+$ T cells in the tumors. We also observed the upregulated expression of PD-1 by intratumoral $CD8^+$ T cells and PD-L1 by tumor cells after polyplex treatment, as part of tumor evasion mechanisms in response to the polyplex vaccine. Based on this phenomenon, we further assessed and demonstrated the synergistic effect between polyplex vaccine and anti-PD-1 therapy. We

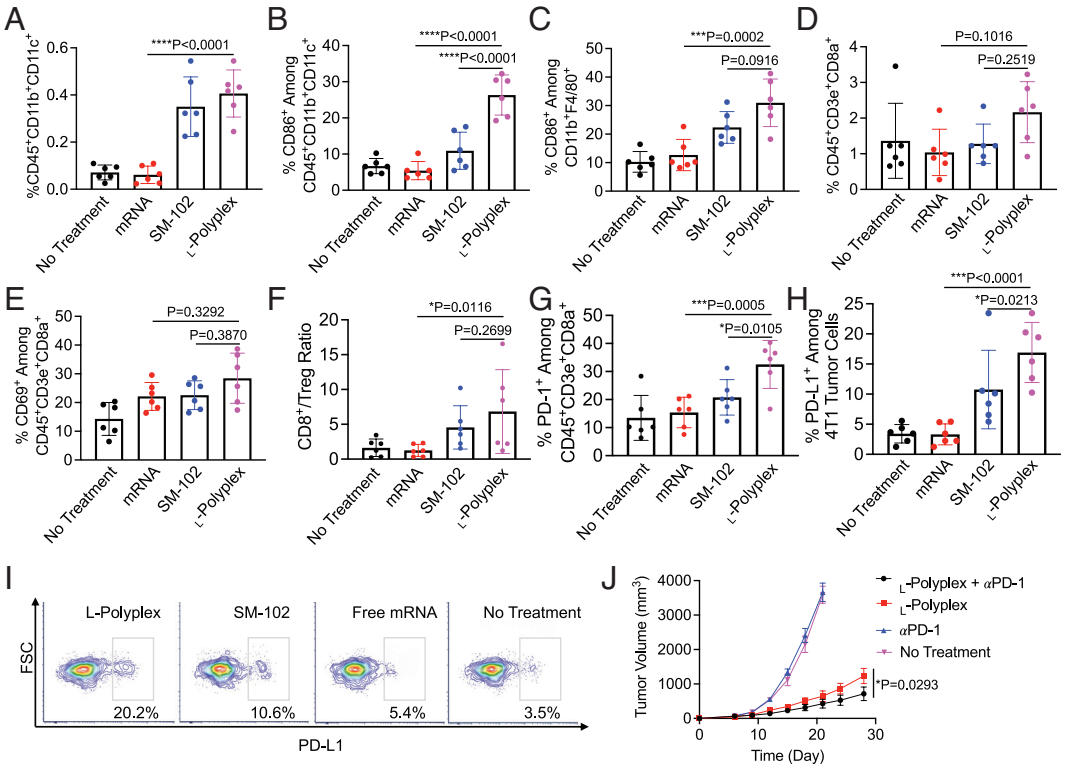

Fig. 6. $PPOB_{50}$-G polyplex reprograms 4T1 tumor microenvironment and synergizes with αPD-1. (*A–I*) 4T1 tumor was inoculated on Day 0. Polyplexes, SM-102 LNP, free mRNA, or PBS were subcutaneously administered on Days 6 and 13 (1 mg/kg mRNA, 4T1-26: 4T1-31: 4T1-32: 4T1-35 = 1:1:1:1). Anti-PD-1 was i.p. injected on Days 14, 16, 18, 20, and 22. (*A*) Percentage of $CD45^+CD11b^+CD11c^+$ DCs in tumors. (*B*) Percentage of $CD86^+$ cells among $CD45^+CD11b^+CD11c^+$ DCs in tumors. (*C*) Percentage of $CD86^+$ cells among $CD45^+CD11b^+F4/80^+$ macrophages in tumors. (*D*) Percentage of $CD45^+CD3e^+CD8a^+$ T cells in tumors. (*E*) Percentage of $CD69^+$ cells among $CD8^+$T cells in tumors. (*F*) $CD8^+$T/Treg number ratios in tumors. Also shown are the percentages of (*G*) $PD\text{-}1^+$ cells among $CD45^+CD3e^+CD8a^+$ T cells and (*H*) $PD\text{-}L1^+$ cells among 4T1 tumor cells. (*I*) Representative FSC-PD-L1 FACS plots of 4T1 tumor cells. (*J*) Average 4T1 tumor volume over time for each group. All the numerical data are presented as mean ± SD except for (*J*) where data are presented as mean ± SEM (for *A–H*, one-way ANOVA with post hoc Fisher's LSD test was used; for (*J*), two-tailed Welch's *t* test was used; $0.01 < {}^*P \le 0.05$; ${}^{**}P \le 0.01$; ${}^{***}P \le 0.001$; ${}^{****}P \le 0.0001$).

anticipate the potential synergy between the polyplex vaccine and other checkpoint blockade therapies, cytokine therapies, and cell therapies.

To conclude, we present a self-adjuvanting α-helical polypeptide that can serve as an effective mRNA carrier and meanwhile properly activate DCs, toward the development of potent mRNA-based cancer vaccines. The cationic α-helical $PPOB_{50}$-G can condense and stabilize neoantigen-encoding mRNAs, facilitate the cellular internalization and translation of mRNAs, and simultaneously upregulate the activation status of DCs. These lead to an enhanced expression and presentation of mRNA-encoded antigens by DCs, and subsequently improve priming of antigen-specific $CD8^+$ T cells. We further demonstrate that the $PPOB_{50}$-G polyplexes can induce potent neoantigen-specific CTL response and antitumor efficacy against 4T1 TNBC, reprogram the immunosuppressive tumor microenvironment, and exhibit synergy with anti-PD-1 therapy. Our polyplex system provides a facile and generalizable platform for the development of robust mRNA-based vaccines for the treatment of different types of tumors, especially poorly immunogenic solid tumors.

Methods

Synthesis of POB-NCA. K_2CO_3 and 4-hydroxybenzyl alcohol were suspended in acetone, followed by the addition of propargyl bromide solution and 18-crown-6. The reaction mixture was refluxed at 75 °C for 12 h. The solvent was then removed and the crude product was resuspended in water and extracted by dichromethane to yield propargyloxybenzyl alcohol. The obtained propargyloxybenzyl alcohol was dissolved in DCM, followed by dropwise addition of thionyl chloride. The obtained propargyloxybenzyl chloride was then added to a mixture of glutamic acid copper (II) complex and 1,1,3,3-tetramethylguanidine in dimethyl formaldehyde. The reaction mixture was stirred at room temperature for 48 h. After washing, the crude product was further purified via recrystallization from isopropanol/water (2:1, v/v) to yield γ-(4-propargyloxybenzyl)-glutamic acid (POB-Glu). POB-Glu was then dissolved in dry THF followed by addition of phosgene. The mixture was refluxed at 50 °C for 2 h. The solvent was removed under vacuum, and the crude product was recrystallized three times in THF/hexane to yield γ-(4-propargyloxybenzyl)-l-glutamic acid *N*-carboxyanhydride (POB- NCA) as white crystals. ^{1}H NMR ($CDCl_3$): δ 7.29 (d, 2H, ArH), 6.98 (d, 2H, ArH), 6.3 (s, 1H, N*H*), 5.08 (s, 2H, ArCH_2–), 4.70 (d, 2H, ArOCH_2–), 4.36 (t, 1H, α-H), 2.55 (m, 3H, –COCH_2CH_2–, *H*C ≡ C–), 2.04 (m, 2H, –CH_2CH_2COO–), 2.29 to 2.10 (m, 2H, –CH_2CH_2COO–).

Synthesis of PPOB. In a glovebox, POB- NCA was dissolved in DMF, followed by the addition of 1-pentylamine. The mixture was stirred at room temperature for 48 h, followed by the removal of DMF under vacuum. The final product PPOB was precipitated with cold methanol and collected as white solid. ^{1}H NMR ($CDCl_3$): δ 7.20 (d, 2H, ArH), 6.86 (d, 2H, ArH), 5.00 to 4.93 (d, 2H, ArCH_2–), 4.58 (s, 2H, ArOCH_2–), 3.98 (s, 1H, α-H), 2.62 to 2.49 (br, 3H, –CH_2CH_2COO–, *H*C ≡ C–), 2.29 to 2.12 (br, 2H, –CH_2CH_2COO–).

Synthesis of PPOB-G. In a glovebox, PPOB, azidohexylguanidine, and *N*,*N*′,*N*″,*N*″-pentamethyldiethylenetriamine were dissolved in DMF. CuBr was then added, and the reaction mixture was stirred at room temperature for 24 h. The final polypeptides were purified by dialysis against water for 3 d (MWCO = 3 kDa) and obtained after lyophilization.

Synthesis of mRNAs. The mRNA encoding SIINFEKL peptide and neoantigen peptides (4T1-26, 4T1-31, 4T1-32, and 4T1-35) were generated using the HiScribe T7 polymerase in vitro transcription system from New England Biolabs (Cat: E2040) following the manufacturer's protocol. The template DNAs used in

the transcription process were obtained from a commercial vendor. Briefly, the template design includes the coding sequence of the peptides, a T7 polymerase recognition sequence, a start codon, a stop codon, and various Untranslated Region sequences. The sequences are appended below this section with the coding regions highlighted in bold. Following in vitro transcription, the mRNA molecules were purified using the Monarch RNA clean up kit from New England Biolabs (Cat: T2050) following the manufacturer's protocol. The concentration and purity of the RNA molecules were determined using the Nanodrop One Spectrophotometer from ThermoScientific (Cat: ND-ONEC-W). The RNA molecules were further analyzed by electrophoresis in a 2% agarose gel prestained with the SYBR Green II from ThermoScientific (Cat: S7564)

Synthesis of Polyplexes. In individual RNase-free Eppendorf tubes, mRNA and polypeptide solutions were separately prepared using Opti-MEM. Subsequently, mRNA and polypeptide with varying N/P ratios were mixed in the RNase-free tubes. The resulting solutions were then incubated in a shaker at 37 °C and shaken at 200 rpm for 30 min.

Synthesis of SM-102 LNP. In RNase-free Eppendorf tube, a lipid mixture in ethanol containing SM-102 (50%), DSPC (10%), cholesterol (38.5%), and PEG-lipid (1.5%) was prepared in ethanol. Separately, mRNA in 25 mM citrate buffer (pH 4.0) was prepared. Then the lipid mixture and mRNA were mixed through the microfluidic cartridge (Microfluidics) at a 3:1 flow rate ratio. After formulation, the mRNA-LNP was dialyzed three times through a 3.5 K MWCO Slide-A-Lyzer dialysis cassette (Thermo Scientific).

Transfection of DCs with Polyplexes. To test the transfection efficiency, 500 ng/mL of mRNA was used across all experiments. Polyplexes were synthesized by mixing SIINFEKL-encoding mRNA or eGFP-encoding mRNA with polypeptides at varied N/P ratios. Lipofectamine 3000 mixed with SIINFEKL-encoding mRNA or eGFP-encoding mRNA were used as controls. BMDCs were then incubated with polyplexes, lipoplexes, free mRNA, and PBS for 16 h. The surface expression of SIINFEKL on BMDCs was assessed by staining cells with fluorophore-conjugated anti-MHCI–SIINFEKL prior to flow cytometry analysis. eGFP-expressing DCs were visualized under a fluorescent microscope or quantified via the flow cytometry. BMDCs were also stained with fluorophore conjugated anti-CD86 and anti-MHCII for the analysis of DC activation status.

Cell Uptake of Polyplexes by DCs. SIINFEKL-encoding mRNAs were stained with SYBR Green II and then complexed with PPOB-G to form the polyplexes. The polyplexes were incubated with DCs for 0.5h and 2 h, respectively, followed by analysis of cells via confocal microscopy and flow cytometry.

Coculture of DCs and OT-1 Cells. To further validate the presentation of SIINFEKL antigen by BMDCs, BMDCs were pretreated with SIINFEKL mRNA polyplexes at varied N/P ratios, lipoplexes, SM-102 LNPs, free mRNA, or PBS for 16 h. DCs were then cocultured with CFSE-stained OT-1 cells (1/1 T cell/DC ratio) for 3 d. The proliferation index of OT-1 cells was then analyzed via flow cytometry.

Polyplex-Mediated Transfection of DCs In Vivo. C57BL/6 mice (5 to 7 wk) were subcutaneously injected (lower flank) with eGFP-encoding polyplexes (10/1 N/P ratio, 1 mg/kg eGFP mRNA). At 0 h, 12 h, 24 h, 48 h, and 72 h, respectively, skin tissue near the injection site and lymph nodes were harvested. Collected tissues were incubated in 1 mg/mL Collagenase Type IV (STEMCELL Technologies, Vancouver, Canada) for 45 min at 37 °C. After the incubation, tissues and lymph nodes were dissociated with a syringe plunger, filtered through a 40 μm cell strainer, and centrifuged. Resulting cell pellets were stained for CD11b, CD11c, CD86, and MHCII for subsequent flow cytometry analysis.

Vaccination Study with mRNA Vaccines. Female C57BL/6 mice (5 to 7 wk) were divided into 5 groups (n = 6 per group): $_{L}$-polyplex, $_{D,L}$-polyplex, lipoplex, free mRNA, and no treatment. For some studies, the SM-102 LNP group substituted the lipoplex group. Polyplexes were prepared by mixing SIINFEKL-encoding mRNA or neoantigen-encoding mRNAs (4T1-26: 4T1-31: 4T1-32: 4T1-35 = 1: 1: 1: 1) with $_{L}$- or $_{D,L}$-polypeptide at 10:1 N/P ratio. mRNA vaccines (1 mg/kg mRNA) were subcutaneously injected into the flank of mice on day 0. On days 7, 14, and 21, blood was collected for the analysis of antigen-specific $CD8^+$ T cells in PBMCs using tetramer staining and IFN-γ restimulation. For tetramer analysis, red blood cells were lysed and cell pellets were stained with APC-conjugated H2Kb-SIINFEKL tetramer, prior to flow cytometry analysis. For IFN-γ restimulation, PBMCs were stimulated with SIINFEKL or neoantigens for 1.5 h, treated with Golgi plug for 2.5 h, and stained with antibodies. Cells were then treated with the fixation & permeabilization buffer and stained with APC-conjugated anti-IFN-γ for flow cytometry analysis. On day 35, a booster vaccine was administered, and antigen-specific $CD8^+$ T cells in PBMCs were analyzed on day 42. For the subsequent prophylactic tumor study, mice were challenged with a subcutaneous injection of E.G7-OVA cells or 4T1 cells. Tumor growth and body weight of animals were closely monitored. The tumor volume was calculated using the formula (length) × $(\text{width})^2/2$, where the long axis diameter was regarded as the length and the short axis diameter was regarded as the width. Mice were euthanized when the largest diameter of tumors reaches 20 mm or mice became moribund.

Therapeutic Tumor Study with mRNA Vaccines. Female C57BL/6 mice (5 to 7 wk) were divided into four groups (n = 6 per group): $_{L}$-polyplex, lipoplex, free mRNA, and no treatment. For some studies, the SM-102 LNP group substituted the lipoplex group. Polyplexes were prepared by mixing SIINFEKL-encoding mRNA or 4T1 neoantigen-encoding mRNAs (4T1-26: 4T1-31: 4T1-32: 4T1-35 = 1: 1: 1: 1) with $_{L}$- or $_{D,L}$-polypeptide at 10:1 N/P ratio. E.G7-OVA or 4T1 cells in Hanks' Balanced Salt Solution were subcutaneously injected into the upper right flank of C57BL/6 mice on day 0. On day 6, when the diameter of tumors reaches ~5 mm, mRNA vaccines (1 mg/kg mRNA) were subcutaneously injected into the lower right flank of mice, followed by a second dose of vaccines on day 13. To evaluate the combination therapy of polyplex vaccines and anti-PD-1, anti-PD-1 (100 μg) was intraperitoneally injected on days 14, 18, 20, 22, and 24. Tumor growth and body weight of animals were closely monitored. The tumor volume was calculated using the formula (length) × $(\text{width})^2/2$, where the long axis diameter was regarded as the length and the short axis diameter was regarded as the width. Mice were euthanized when the largest diameter of tumors reaches 20 mm or mice became moribund. Mice were monitored for at least 200 d to ensure they are tumor-free.

Tumor Microenvironment Analysis. 4T1 cells were subcutaneously injected into the flank of female Balb/c mice (5 to 7 wk). After the tumors were established, mice were randomly divided into four groups (n = 6 per group): $_{L}$-polyplex, SM-102 LNP, free mRNA, and no treatment. On day 6 and day 13, mRNA vaccines (1 mg/kg mRNA) were subcutaneously injected into the lower right flank of mice. On day 27, tumors were harvested for analysis. Tumors were incubated with collagenase for 45 min at 37 °C, disrupted, and filtered through a 40 μm cell strainer. The cell pallets were stained with antibodies prior to flow cytometry analysis.

Statistical Analyses. Statistical analysis was performed using GraphPad Prism v6 and v8. Sample variance was tested using the F test. For samples with equal variance, the significance between the groups was analyzed by a two-tailed Student's *t* test. For samples with unequal variance, a two-tailed Welch's *t* test was performed. For multiple comparisons, a one-way ANOVA with post hoc Fisher's LSD test was used. The results were deemed significant at $0.01 < {}^*P \le 0.05$, $0.001 < {}^{**}P \le 0.01$, highly significant at $0.0001 < {}^{***}P \le 0.001$, and extremely significant at $^{****}P \le 0.0001$.

Statistics and Reproducibility. The sample sizes were determined empirically. In general, in vitro studies involve n = 3 to 6 and in vivo studies involve n = 6. No data were excluded from the analyses. Randomization was used for animal studies.

Data, Materials, and Software Availability. Raw data will be publicly available in a repository in Illinois Data Bank upon publication. DOI: https://databank.illinois.edu/datasets/IDB-0680730 (60).

ACKNOWLEDGMENTS. We would like to acknowledge the financial support from NSF Division of Materials Research 21-43673 CAR (H.W.), NIH R01CA274738 (H.W.), Sontag Distinguished Scientist Award (H.W.), and American Cancer Society Research Scholar Award (H.W.). This material is based upon work supported by the Air Force Office of Scientific Research under award number FA9550-23-1-0609 (Q.C. and H.W.).

Author affiliations: [a]Department of Materials Science and Engineering, University of Illinois at Urbana-Champaign, Urbana, IL 61801; [b]Department of Bioengineering, University of Illinois at Urbana-Champaign, Urbana, IL 61801; [c]Department of Veterinary Clinical Medicine, University of Illinois at Urbana-Champaign, Urbana, IL 61801; [d]Alnylam Pharmaceuticals, Inc., Cambridge, MA 02142; [e]Cancer Center at Illinois, Urbana, IL 61801; [f]Carle College of Medicine, University of Illinois at Urbana-Champaign, Urbana,

IL 61801; [g]Zhejiang University-University of Edinburgh Institute, Zhejiang University School of Medicine, International Campus, Zhejiang University, Haining 314400, China; [h]Department of Chemistry, University of Illinois at Urbana-Champaign, Urbana, IL 61801; [i]Beckman Institute for Advanced Science and Technology, University of Illinois at Urbana-Champaign, Urbana, IL 61801; [j]Materials Research Laboratory, University of Illinois at Urbana-Champaign, Urbana, IL 61801; [k]Department of Electrical and Computer Engineering, University of Illinois at Urbana-Champaign, Urbana, IL 61801; and [l]Institute for Genomic Biology, University of Illinois at Urbana-Champaign, Urbana, IL 61801

Author contributions: J.H. and H.W. designed research; J.H., J.Z., A.D., T.X., R.B., Y.L., D.N., Y.B., Y.W., Xin Wang, M.X., M.B., K.B., J.I., J.L., Q.C., S.N., and Xing Wang performed research; J.H., J.Z., A.D., T.X., R.B., Y.L., D.N., Y.B., Y.W., M.X., M.B., K.B., J.I., J.L., Q.C., S.N., Xing Wang, and H.W. analyzed data; and J.H. and H.W. wrote the paper.

Competing interest statement: H.W. and J.H. filed a patent application for the self-adjuvanting α-helical polypeptides based mRNA cancer vaccines. Other authors declare no competing interests.

1. I. Mellman, G. Coukos, G. Dranoff, Cancer immunotherapy comes of age. *Nature* **480**, 480–489 (2011).
2. W. J. Lesterhuis, J. B. Haanen, C. J. Punt, Cancer immunotherapy–revisited. *Nat. Rev. Drug Discov.* **10**, 591–600 (2011).
3. R. S. Riley, C. H. June, R. Langer, M. J. Mitchell, Delivery technologies for cancer immunotherapy. *Nat. Rev. Drug Discov.* **18**, 175–196 (2019).
4. A. Ribas, J. D. Wolchok, Cancer immunotherapy using checkpoint blockade. *Science* **359**, 1350–1355 (2018).
5. R. N. Amaria *et al.*, Neoadjuvant immune checkpoint blockade in high-risk resectable melanoma. *Nat. Med.* **24**, 1649–1654 (2018).
6. R. C. Sterner, R. M. Sterner, CAR-T cell therapy: Current limitations and potential strategies. *Blood Cancer J.* **11**, 69 (2021).
7. N. N. Shah, T. J. Fry, Mechanisms of resistance to CAR T cell therapy. *Nat. Rev. Clin. Oncol.* **16**, 372–385 (2019).
8. M. A. Postow, R. Sidlow, M. D. Hellmann, Immune-related adverse events associated with immune checkpoint blockade. *N. Engl. J. Med.* **378**, 158–168 (2018).
9. S. Rafiq, C. S. Hackett, R. J. Brentjens, Engineering strategies to overcome the current roadblocks in CAR T cell therapy. *Nat. Rev. Clin. Oncol.* **17**, 147–167 (2020).
10. M. Saxena, S. H. van der Burg, C. J. Melief, N. Bhardwaj, Therapeutic cancer vaccines. *Nat. Rev. Cancer* **21**, 360–378 (2021).
11. C. J. Melief, T. van Hall, R. Arens, F. Ossendorp, S. H. van der Burg, Therapeutic cancer vaccines. *J. Clin. Invest.* **125**, 3401–3412 (2015).
12. D. J. Irvine, Materializing the future of vaccines and immunotherapy. *Nat. Rev. Mater.* **1**, 1–2 (2016).
13. D. J. Irvine, M. A. Swartz, G. L. Szeto, Engineering synthetic vaccines using cues from natural immunity. *Nat. Mater.* **12**, 978–990 (2013).
14. S. A. Rosenberg, J. C. Yang, N. P. Restifo, Cancer immunotherapy: Moving beyond current vaccines. *Nat. Med.* **10**, 909–915 (2004).
15. S. Kreiter *et al.*, Mutant MHC class II epitopes drive therapeutic immune responses to cancer. *Nature* **520**, 692–696 (2015).
16. L. Miao, Y. Zhang, L. Huang, mRNA vaccine for cancer immunotherapy. *Mol. Cancer* **20**, 1–23 (2021).
17. U. Sahin *et al.*, Personalized RNA mutanome vaccines mobilize poly-specific therapeutic immunity against cancer. *Nature* **547**, 222–226 (2017).
18. J. Chen *et al.*, Lipid nanoparticle-mediated lymph node–targeting delivery of mRNA cancer vaccine elicits robust CD8+ T cell response. *Proc. Natl Acad. Sci. U.S.A.* **119**, e2207841119 (2022).
19. R. Yao, C. Xie, X. Xia, Recent progress in mRNA cancer vaccines. *Hum. Vaccin. Immunother.* **20**, 2307187 (2024).
20. L. A. Rojas *et al.*, Personalized RNA neoantigen vaccines stimulate T cells in pancreatic cancer. *Nature* **618**, 144–150 (2023).
21. J. S. Weber *et al.*, Individualised neoantigen therapy mRNA-4157 (V940) plus pembrolizumab versus pembrolizumab monotherapy in resected melanoma (KEYNOTE-942): A randomised, phase 2b study. *Lancet* **403**, 632–644 (2024).
22. R. T. Shroff *et al.*, Immune responses to two and three doses of the BNT162b2 mRNA vaccine in adults with solid tumors. *Nat. Med.* **27**, 2002–2011 (2021).
23. C. D. Palmer *et al.*, Individualized, heterologous chimpanzee adenovirus and self-amplifying mRNA neoantigen vaccine for advanced metastatic solid tumors: Phase 1 trial interim results. *Nat. Med.* **28**, 1619–1629 (2022).
24. O. Bechter *et al.*, 391 A first-in-human study of intratumoral SAR441000, an mRNA mixture encoding IL-12sc, interferon alpha2b, GM-CSF and IL-15sushi as monotherapy and in combination with cemiplimab in advanced solid tumors. *J. Immunother. Cancer* **8**, (2020). https://doi.org/10.1136/jitc-2020-SITC2020.0391.
25. U. Sahin, Ö. Türeci, Personalized vaccines for cancer immunotherapy. *Science* **359**, 1355–1360 (2018).
26. M. A. Oberli *et al.*, Lipid nanoparticle assisted mRNA delivery for potent cancer immunotherapy. *Nano Lett.* **17**, 1326–1335 (2017).
27. H. Zhang *et al.*, Delivery of mRNA vaccine with a lipid-like material potentiates antitumor efficacy through Toll-like receptor 4 signaling. *Proc. Natl. Acad. Sci. U.S.A.* **118**, e2005191118 (2021).
28. L. Miao *et al.*, Delivery of mRNA vaccines with heterocyclic lipids increases anti-tumor efficacy by STING-mediated immune cell activation. *Nat. Biotechnol.* **37**, 1174–1185 (2019).
29. J. Ramos da Silva *et al.*, Single immunizations of self-amplifying or non-replicating mRNA-LNP vaccines control HPV-associated tumors in mice. *Sci. Transl. Med.* **15**, eabn3464 (2023).
30. X. Hou, T. Zaks, R. Langer, Y. Dong, Lipid nanoparticles for mRNA delivery. *Nat. Rev. Mater.* **6**, 1078–1094 (2021).
31. K. A. Hajj, K. A. Whitehead, Tools for translation: Non-viral materials for therapeutic mRNA delivery. *Nat. Rev. Mater.* **2**, 1–17 (2017).
32. P. S. Kowalski, A. Rudra, L. Miao, D. G. Anderson, Delivering the messenger: Advances in technologies for therapeutic mRNA delivery. *Mol. Ther.* **27**, 710–728 (2019).
33. A. J. Barbier, A. Y. Jiang, P. Zhang, R. Wooster, D. G. Anderson, The clinical progress of mRNA vaccines and immunotherapies. *Nat. Biotechnol.* **40**, 840–854 (2022).
34. U. Sahin, K. Karikó, Ö. Türeci, mRNA-based therapeutics–Developing a new class of drugs. *Nat. Rev. Drug Discov.* **13**, 759–780 (2014).
35. P. Huang *et al.*, An integrated polymeric mRNA vaccine without inflammation side effects for cellular immunity mediated cancer therapy. *Adv. Mater.* **35**, 2207471 (2023).
36. L. Miao, Y. Zhang, L. Huang, mRNA vaccine for cancer immunotherapy. *Mol. Cancer* **20**, 41 (2021).
37. E. Ben-Akiva *et al.*, Biodegradable lipophilic polymeric mRNA nanoparticles for ligand-free targeting of splenic dendritic cells for cancer vaccination. *Proc. Natl. Acad. Sci. U.S.A.* **120**, e2301606120 (2023).
38. X. Liu, P. Huang, R. Yang, H. Deng, mRNA cancer vaccines: Construction and boosting strategies. *ACS Nano* **17**, 19550–19580 (2023).
39. M. Lindgren, M. Hällbrink, A. Prochiantz, Ü. Langel, Cell-penetrating peptides. *Trends Pharmacol. Sci.* **21**, 99–103 (2000).
40. G. Guidotti, L. Brambilla, D. Rossi, Cell-penetrating peptides: From basic research to clinics. *Trends Pharmacol. Sci.* **38**, 406–424 (2017).
41. F. Milletti, Cell-penetrating peptides: Classes, origin, and current landscape. *Drug Discov. Today* **17**, 850–860 (2012).
42. B. Zhao *et al.*, Development of polypeptide-based materials toward messenger RNA delivery. *Nanoscale* **16**, 2250–2264 (2024).
43. H. Lu *et al.*, Ionic polypeptides with unusual helical stability. *Nat. Commun.* **2**, 206 (2011).
44. M. Xiong *et al.*, Helical antimicrobial polypeptides with radial amphiphilicity. *Proc. Natl. Acad. Sci. U.S.A.* **112**, 13155–13160 (2015).
45. H.-X. Wang *et al.*, Nonviral gene editing via CRISPR/Cas9 delivery by membrane-disruptive and endosomolytic helical polypeptide. *Proc. Natl. Acad. Sci. U.S.A.* **115**, 4903–4908 (2018).
46. J. Yen *et al.*, Cationic, helical polypeptide-based gene delivery for IMR-90 fibroblasts and human embryonic stem cells. *Biomater. Sci.* **1**, 719–727 (2013).
47. Z. Song *et al.*, Secondary structures in synthetic polypeptides from N-carboxyanhydrides: Design, modulation, association, and material applications. *Chem. Soc. Rev.* **47**, 7401–7425 (2018).
48. N. P. Gabrielson *et al.*, Reactive and bioactive cationic α-helical polypeptide template for nonviral gene delivery. *Angew. Chem. Int. Ed. Engl.* **124**, 1169–1173 (2012).
49. N. P. Gabrielson, H. Lu, L. Yin, K. H. Kim, J. Cheng, A cell-penetrating helical polymer for siRNA delivery to mammalian cells. *Mol. Ther.* **20**, 1599–1609 (2012).
50. H. Wang *et al.*, Biomaterial-based scaffold for in situ chemo-immunotherapy to treat poorly immunogenic tumors. *Nat. Commun.* **11**, 5696 (2020).
51. H. Wang *et al.*, Metabolic labeling and targeted modulation of dendritic cells. *Nat. Mater.* **19**, 1244–1252 (2020).
52. L. Ohl *et al.*, CCR7 governs skin dendritic cell migration under inflammatory and steady-state conditions. *Immunity* **21**, 279–288 (2004).
53. J. Han *et al.*, Metabolic glycan labeling immobilizes dendritic cell membrane and enhances antitumor efficacy of dendritic cell vaccine. *Nat. Commun.* **14**, 5049 (2023), 10.1038/s41467-023-40886-7.
54. C. L. Lorentzen, J. B. Haanen, Ö. Met, I. M. Svane, Clinical advances and ongoing trials on mRNA vaccines for cancer treatment. *Lancet Oncol.* **23**, e450–e458 (2022).
55. E. Kon, N. Ad-El, I. Hazan-Halevy, L. Stotsky-Oterin, D. Peer, Targeting cancer with mRNA–lipid nanoparticles: Key considerations and future prospects. *Nat. Rev. Clin. Oncol.* **20**, 739–754 (2023).
56. M. Skwarczynski *et al.*, Poly(amino acids) as a potent self-adjuvanting delivery system for peptide-based nanovaccines. *Sci. Adv.* **6**, eaax2285 (2020).
57. V. K. Udhayakumar *et al.*, Arginine-rich peptide-based mRNA nanocomplexes efficiently instigate cytotoxic T cell immunity dependent on the amphipathic organization of the peptide. *Adv. Healthcare Mater.* **6**, 1601412 (2017).
58. S. Lei *et al.*, ALPPL2-binding peptide facilitates targeted mRNA delivery for efficient hepatocellular carcinoma gene therapy. *Adv. Funct. Mater.* **32**, 2204342 (2022).
59. K. A. Pilones *et al.*, Invariant natural killer T cells regulate breast cancer response to radiation and CTLA-4 blockade. *Clin. Cancer Res.* **15**, 597–606 (2009).
60. H. Wang, J. Han, Self-adjuvanting α-helical polypeptide simultaneously delivers neoantigen mRNAs and activates dendritic cells to eradicate tumors. Illinois Data Bank. https://databank.illinois.edu/datasets/IDB-0680730. Deposited 1 April 2026.